LANGMUIR

pubs.acs.org/Langmuir Article

Observing Real-Time Adhesion of Microparticles on Glass Surfaces

Pillalamarri Srikrishnarka, Dhivyaraja Kumaran, Amoghavarsha Ramachandra Kini, Vishal Kumar, Ankit Nagar, Md Rabiul Islam, Ramamurthy Nagarajan,* and Thalappil Pradeep*

Cite This: https://doi.org/10.1021/acs.langmuir.3c01856 Read Online

ACCESS | Metrics & More | Article Recommendations | Supporting Information

ABSTRACT: Fouling on glass surfaces reduces the solar panel efficiency and increases water consumption for cleaning. Superhydrophobic coatings on glass enable self-cleaning by allowing water droplets to carry away dirt particles. Observing the interaction between charged particles and surfaces provides insights into effective cleaning. Using a high-speed camera and a long-distance objective, we analyzed the *in situ* deposition of variously functionalized and charged silica dust microparticles on chemically treated glass. The ambient charges for the control, hydrophobic, and positively charged particles were approximately −0.5, −0.13, and +0.5 nC, respectively. We found that a positively charged particle of 2.3 ± 1.2 μm diameter adhered to hydroxylated glass in ∼0.054 s, compared to 0.40 and 0.45 s for quaternary ammonium- and fluorosilane-functionalized hydrophobic glass. Experiments suggest that quaternary ammonium-functionalized glass surfaces are about 77.8% more resistant to soiling than bare surfaces.

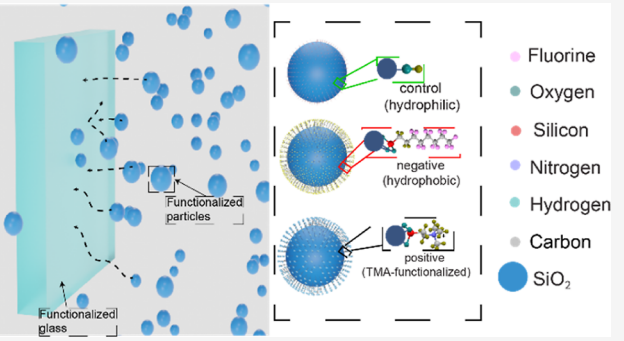

INTRODUCTION

Dust buildup on photovoltaic (PV) panels and façades is a severe problem since it negatively impacts light transmission and performance, including energy conversion efficiency. Also, large volumes of water are used in cleaning these surfaces. Dust travels long distances ranging from a few meters to thousands of kilometers, impacting the local environment and human health.[1] According to Elminir et al., dust deposited on horizontally installed PV panels in arid environments was ∼15.84 g m^{-2}, resulting in a 52.5% decrease in light transmission.[2] Panat and Varanasi observed that with 50 g m^{-2} dust deposition, there was ∼50% loss in a solar panel's power output at a lab scale, under simulated harsh soiling.[3] A global economic loss of between 3.3 and 5.5 billion USD is caused by an average power loss of 3 to 4%.[4] A 1 MW solar farm requires close to 24,000 L of water or roughly 3−4 L per solar panel of ∼400 W for cleaning. Moon et al. showed that even the most effective robotic cleaning system requires ∼570 L of water to clean an area of 3000 m^2 (amounting to 5221 W) in an hour.[5] Dust deposition on PV panels is dynamic, and it depends on the location. Such particles could be natural or anthropogenic in origin.[6,7] These particles affect the quality of air[8,9] and consequently impact the local environment.

Inspired by nature, glass surfaces have been treated with transparent superhydrophobic coatings such as fluorosilane[10−13] and nonfluorinated silane[14−16] to remove dust particles passively. Recently, Dhar et al. reported a transparent superhydrophobic coating using dipentaerythritol pentaacrylate reacted with branched polyethylenimine which was spray-coated on glass to impart hydrophobicity.[17] Due to this superhydrophobic coating, a water flow removed the deposited model dust particles.[17] Zhang and Seegar fabricated a new group of nanostructures based on silicone nanofilaments.[18] These filaments were grown on glass and immersed in a toluene solution, and their growth was controlled by regulating water concentration during the condensation of trichlorosilane. These filaments were treated with O_2 plasma and modified with 1H, 1H, 2H, and 2H-perfluoro-decyl trichlorosilane. This transformed it into a superhydrophobic surface with excellent transparency. Ganesh et al. fabricated a superhydrophobic coating on glass using electrospinning to remove dirt without compromising transparency.[19−21] Active cleaning methods are being investigated to curb excessive water use and to transition to sustainable cleaning systems.[22] Some of the useful techniques include superhydrophobic coatings on glass surfaces, electrostatic cleaning, straightforward brushing, and ultrasonic cleaning. With the assistance of hydrophilic curved rings on a hydrophobic backdrop, Sun and Böhringer produced an active self-cleaning system capable of eliminating all types of dust particles from the surface. Here, mechanical vibrations were utilized to remove dust particles in the

Received: July 4, 2023
Revised: October 26, 2023
Accepted: October 27, 2023

presence of water as they trickled down the surface.[23] Vagra and Wiesner utilized a centrifugal force of ∼65.9 nN to dislodge silica particles in the size range of ∼15 to 30 μm from a glass surface.[24] Recently, Kawamoto and co-workers installed parallel electrodes on the surface of PV panels connected to a high-voltage AC supply. When the panel was tilted and the electrodes were switched between positive and negative potentials alternatively at regular intervals, the resulting electrostatic forces made the dust particles fall, cleaning the surface without water.[25] A similar approach was followed by Panat and Varanasi, where they observed high removal efficiency even using a DC voltage and successfully recovered ∼95% of the lost power after cleaning.[3] Wang et al. fabricated a superhydrophobic antireflective coating on the PV module, which self-cleaned under artificial rain, providing a new approach to clean large-scale PV farms due to its cost-effectiveness and scalability.[26] The methods mentioned above remove particles with a size >30 μm, but the removal efficiency decreases for fine and ultrafine particles. Upon adhesion, these particles will further aggregate and degrade the overall performance of the solar panels. Therefore, avoiding particle adherence as well as removing them early is important from multiple perspectives.

Superhydrophobic surfaces have varied applications including oil/water separation,[27] eco-friendly clothing, etc. For example, a cotton fabric was coated with appropriate molecular coatings for hydrophobicity.[28] This fabric[28] was superhydrophobic and superoleophilic with an oil/water separation efficiency of 98.49% even after 18 cycles. A multifunctional fabric which is superhydrophobic with properties such as thermal stability even at 180 °C, pH stability, resistance to organic solvents, and abrasion resistance was fabricated using a polyethylene terephthalate (PET) fabric with hierarchical structures by in situ polymerization of pyrrole over it.[29] Further treatment of this fabric with pentaerythritol tetraacrylate, 3-aminopropyltriethoxysilane, and octadecyl acrylate imparted multifunctionality to this fabric. Superhydrophobic fabrics also help build wearable sensors, especially for monitoring sweat rate and its composition.[30,31] Recently, Liu et al. fabricated a sweat sensor based on polyacrylate sodium/MXene which was further sandwiched between two superhydrophobic textile layers for monitoring sweat vapor with high sensitivity and rapid response time.[32] The superhydrophobic fabric enabled excellent breathability for the permeation of water vapor and prevented the sensor from external water droplets and internal sensible sweat.

In this paper, we present a study of the interaction between microscopic model dust particles and functionalized glass surfaces in real time. The particles were tracked using the image sequence obtained from a high-speed camera, and we found that hydrophobic glass foul less than the hydrophilic ones. Particles tend to deposit faster on hydrophilic glass than on hydrophobic or amine-functionalized glass. Surface energy and charge could increase the time needed for particle adhesion. The methodology presented could help evaluate dust adhesion on glass and help in assessing the ease of cleaning for a specific type of glass. To the best of our knowledge, there has been no report on such time-resolved observations of particle adhesion on surfaces.

■ MATERIALS AND METHODS

Materials. Ethanol (absolute AR) and hexane were purchased from Fisher Scientific UK, and sulfuric acid (AR) (H_2SO_4) was purchased from RANKEM, India. 1H, 1H, 2H, 2H- perfluorooctyltriethoxysilane (98%) (PTFS) and hydrogen peroxide (H_2O_2) were purchased from Sigma-Aldrich, India. *N*-Trimethoxysilylpropyl-*N*,-*N*,-*N*-trimethylammonium chloride (TMA) was purchased from TCL Chemicals India Pvt. Ltd. Microscopic glass slides (75 × 25 × 1.3) mm^2 were from BLUE STAR, India, and spherical silica particles (SS-T-2.5, 1−5 μm) were from Sinoenergy Corporation, China. Millipore-produced deionized (DI) water was used throughout the experiments, and all the reagents were used without further purification.

Methods. *Functionalization of Glass.* The glass slides were cleaned before further surface functionalization. A three-step process was followed for cleaning these glass slides; initially, the glass slides were cut to dimensions of 28 × 25 mm^2 using a diamond cutter. The cut-glass slides were sonicated for 15 min in soap solution. After washing, they were sonicated in ethanol for another 15 min. Finally, they were immersed in piranha solution [1:4 (v/v) 30% H_2O_2 and 30% H_2SO_4] for 2 h. Following this, glass slides were rinsed with DI water and finally dried by using dry nitrogen (N_2) gas. To transform these hydrophilic glass slides into hydrophobic ones, the glass slides were immersed in 1 mM PTFS hexane solution for 12 h. These slides were rinsed with hexane to remove any unbound PTFS and the hydrophobic glass slides so formed were dried under N_2 gas. To impart positive charges on the glass, the hydrophilic glass slides were immersed in a 1 mM ethanol solution of TMA for 12 h. Slides were rinsed with ethanol to remove any unbound TMA and dried using N_2 gas.

Functionalization of Particles. About 10 g of silica particles was added to a soap solution and sonicated for 15 min, following which, they were vacuum-filtered and washed twice with DI water. These particles were further added to an ethanol solution, sonicated for 15 min, and vacuum-filtered. The filtered particles were transferred to a piranha solution for 2 h. Finally, the particles were rinsed with DI water, vacuum-filtered one more time, and dried in an oven at 75 °C overnight. From these dried particles, about 3 g was later transferred to 1 mM PTFS in hexane and kept for 12 h to impart hydrophobicity. They were vacuum-filtered, dried overnight, and transferred to polypropylene (PP) bottles for later use. Similarly, another 3 g of the dried particles was transferred to 1 mM TMA ethanol solution for 12 h to impart the amine functionality.[33] These particles were washed with ethanol, dried, and transferred to a PP bottle. The remaining hydrophilic silica particles were transferred to a PP bottle for further use.

Ambient Dust Deposition. To visualize the ambient dust deposited on different glasses, functionalized glasses were vertically placed at the top of a ∼20 m high building within the academic zone of the Indian Institute of Technology (IIT) Madras, Chennai, India. The glass slides were placed during the summer months, and at the end of each day, the slides were visualized under an optical microscope to note the ambient particle deposition.

Model Dust Deposition. For investigating the model dust deposition on functionalized glass, the experiment was conducted in an acrylic chamber. The silica particles were fluidized by using a medical-grade nebulizer operating at a fixed flow rate of 0.4 mL min^{-1}. The flow of these particles was stopped after 5 s, following which the glass slides were removed and the particle distribution on the surface was plotted.

Feret Diameter Measurement. To measure the diameter of the particle and calculate the size distribution, the Feret diameter was measured by using a custom MATLAB function. Briefly, the image of interest was chosen from which a specific region was selected by cropping the unwanted parts. The color image was then transformed into a binary image, and "fill holes" functionality was used to fill any gaps. Then the Feret diameter was measured using the "Feret diameter" function in MATLAB. Then each diameter was multiplied with a scale of 0.7 μm $pixel^{-1}$ and the distribution was plotted as a histogram. The corresponding code is presented as Annexure-1.

In Situ Particle−Surface Interactions. To investigate particle−surface interactions, a glass slide was placed vertically inside a transparent acrylic chamber of dimensions 10 × 10 × 10 cm^3, having an inlet and outlet for the flow of silica particles. The glass was placed

https://doi.org/10.1021/acs.langmuir.3c01856
Langmuir XXXX, XXX, XXX−XXX

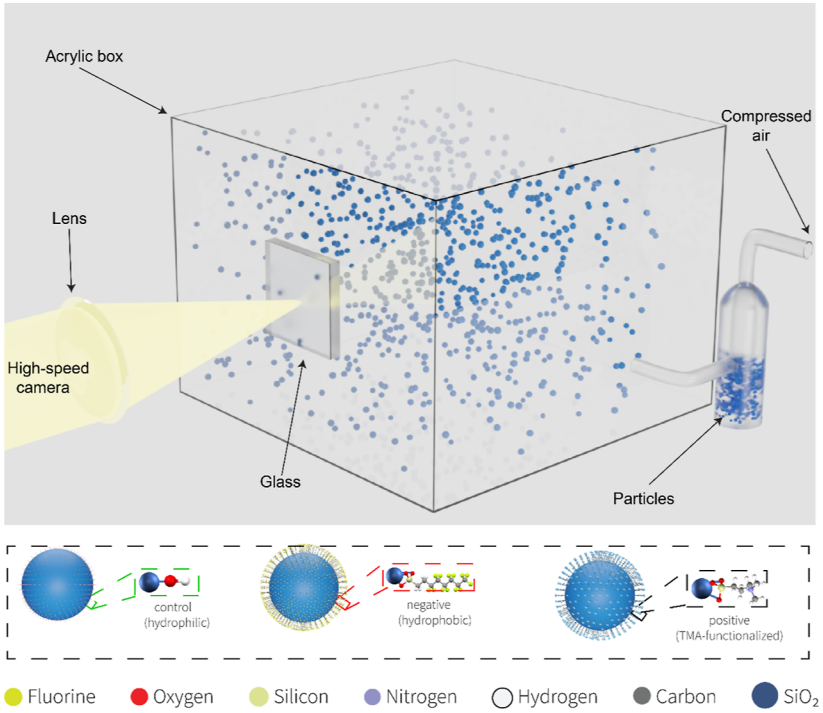

Figure 1. Schematic representation of the experimental setup and molecular models of functionalized silica particles are shown in the inset below. Fluidized microparticles of different functionalities impacting the glass slide randomly are imaged by a high-speed camera.

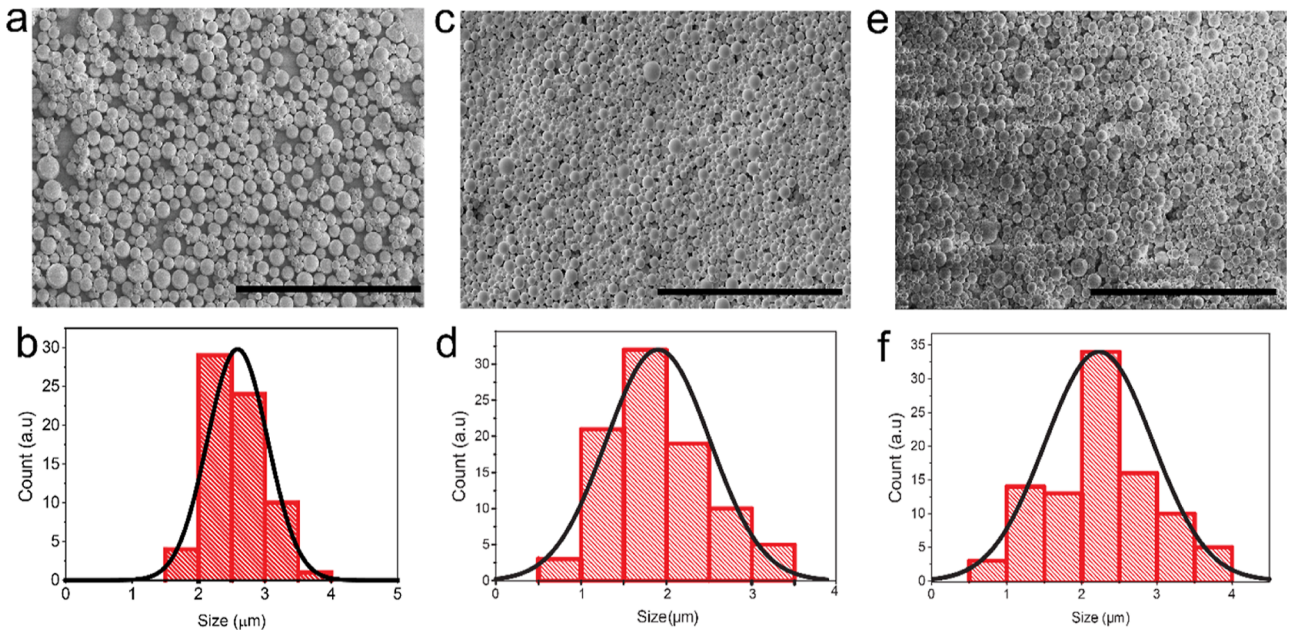

Figure 2. (a,c,e) Scanning electron micrographs of bare, hydrophobic (PTFS), and positively charged (TMA)-treated silica particles with a scale bar of 20 μm. (b,d,f) Corresponding size distribution of the silica particles measured from SEM.

vertically at the center of the acrylic chamber. This acrylic chamber was placed on a Labjack (Holmarc), which was further placed on an optical rail (Thorlabs). These were then placed on an optical table with vibration isolation. A schematic of the acrylic chamber hosting the glass slide and particles is shown in Figure 1. Silica particles were fluidized using precleaned compressed air obtained from a medical-grade nebulizer with a flow rate of 0.4 mL min^{-1}. A gas trap with a flat base was used to contain the silica particles. Gas was let in from the top of the trap to fluidize the particles, and from the side, these particles were transported inside the acrylic chamber as shown in Figure 1. A high-speed camera (Phantom V1212, 1000 frames per s) was coupled with a long-working distance objective (KEYENCE ZHX 1000×) viewed at 1000× magnification. A frame size of 536 × 496 pixels with a resolution of ~0.7 μm pixel^{-1} was obtained from calibration images. A continuous 300 W Xe arc lamp was coupled to the zoom lens in the coaxial illumination mode to illuminate the foreground and increase the sharpness of the particles deposited on the glass slide. The background was illuminated by using a Veritas Constellation 120E LED strobe light, operating in continuous mode at 120 W. The acrylic chamber was placed in such a way that the focal point of the lens was exactly on the glass facing the particles. The experiments were conducted at 18 °C and at 35%RH. The low

https://doi.org/10.1021/acs.langmuir.3c01856
Langmuir XXXX, XXX, XXX−XXX

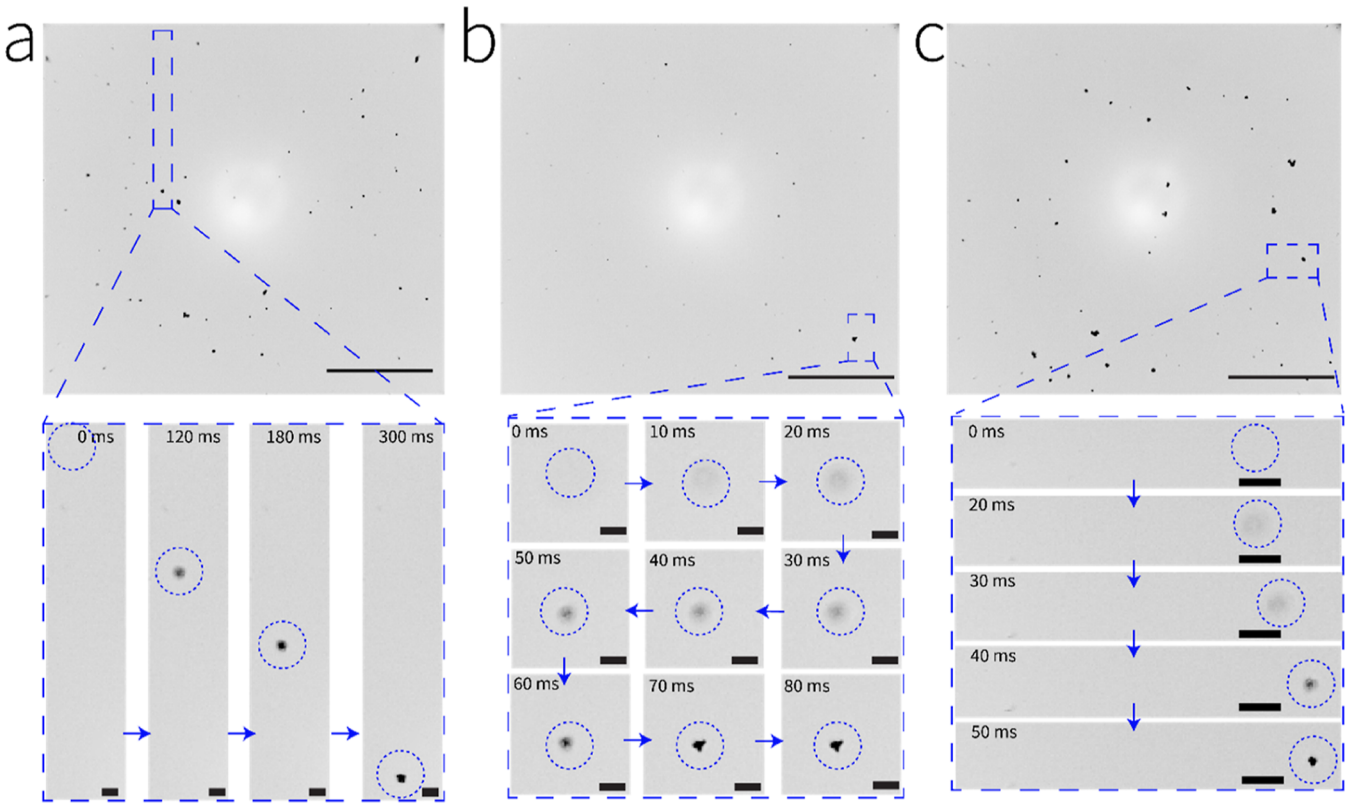

Figure 3. Digital photographs were taken from a high-speed camera. The interaction of positive, control, and negatively charged particles on hydrophilic glass is shown in (a, b, and c, respectively). The scale bar corresponds to 100 μm. In all the magnified images in the bottom frames, the scale bar corresponds to 10 μm. Dotted circles correspond to the particles of interest.

temperature was needed to protect the high-speed camera, strobe light, and Xe arc lamp from overheating.

CHARACTERIZATION

Silica particles were characterized with a Thermo Scientific Verios G4 UC FESEM, with retractable detectors operating at 2 kV. The samples were gold sputtered using a CRESSINGTON sputter coater operating for a period of 80 s. Glass slides after exposure to silica particles were viewed with a Leica polarization microscope for particle counting. The Feret diameter was noted by using MATLAB 20 software. The functionalized silica particles and glass slides were characterized using a Thermo Scientific Spectrum one FTIR instrument operated in the total attenuated reflection (ATR) mode to confirm the presence of the hydrophobic and amine moieties. The coatings on the glass after multiple cycles of modification and washing of the glass slides were confirmed with X-ray photoelectron spectroscopy (XPS). This analysis was carried out by using an Omicron ESCA probe TPD with Al Kα as the X-ray source (1486.86 eV). Survey scans were performed at a pass energy of 50 eV and a step size of 0.5 eV, ranging from 0 to 1100 eV binding energy, to identify all the elements in the samples. Detailed scans were conducted for the elements of interest at a pass energy of 20 eV and a step size of 0.08 eV. In order to obtain the best resolution of the peaks, detailed scans for the elements of interest were run at least three times each. Contact angle measurements were performed by using the sessile droplet method, with water being used as the solvent (with a volume of 3 μL) using a Holmarc contact angle meter. To measure the ambient charge of the particles, about 10 mg of the particles was added to a Faraday cup that was connected to a Keithley 6514 electrometer.

RESULTS AND DISCUSSION

Fabrication of Model Dust and Functionalized Glass. For creating model dust particles, spherical silica particles (size 2.5 ± 1.2 μm as seen in Figure 2c) were functionalized with PTFS to impart hydrophobicity and TMA to impart positive charges. The particles are spherical as seen in Figure 2a and have a size of 2.5 ± 1.5 μm as shown in Figure 2b. Scanning electron micrographs of the negatively and positively charged particles are shown in Figure 2c,e. The size of negatively and positively charged particles was 2.3 ± 1.2 and 2.4 ± 0.6 μm, respectively, as shown in Figure 2d,f. There were no artifacts and surface deformations observed and the particles remained spherical even after chemical functionalization.

FTIR analysis was performed to confirm these moieties on silica particles, and a comparison of the data is shown in Figure S1. The peaks at 1138 and 1190 cm^{-1} confirm the presence of CF_3 and CF_2 vibrations in the hydrophobic silica. A peak at 1214 cm^{-1} is attributed to C−N stretching, confirming the anchoring of the amine moieties. A summary of the FTIR peaks is presented in Table S1.

About 100 mg of untreated, hydrophobic, and TMA-functionalized silica particles were added to a Faraday cup which was in turn connected to a Keithley 6510 electrometer. Figure S2 shows the ambient charge of particles as soon as they were added to the Faraday cup. Bare silica particles had a charge of −0.5 nC, hydrophobic silica particles had a charge of −0.13 nC, and TMA-functionalized particles had a charge of +0.5 nC due to the presence of the amine group. This

https://doi.org/10.1021/acs.langmuir.3c01856
Langmuir XXXX, XXX, XXX−XXX

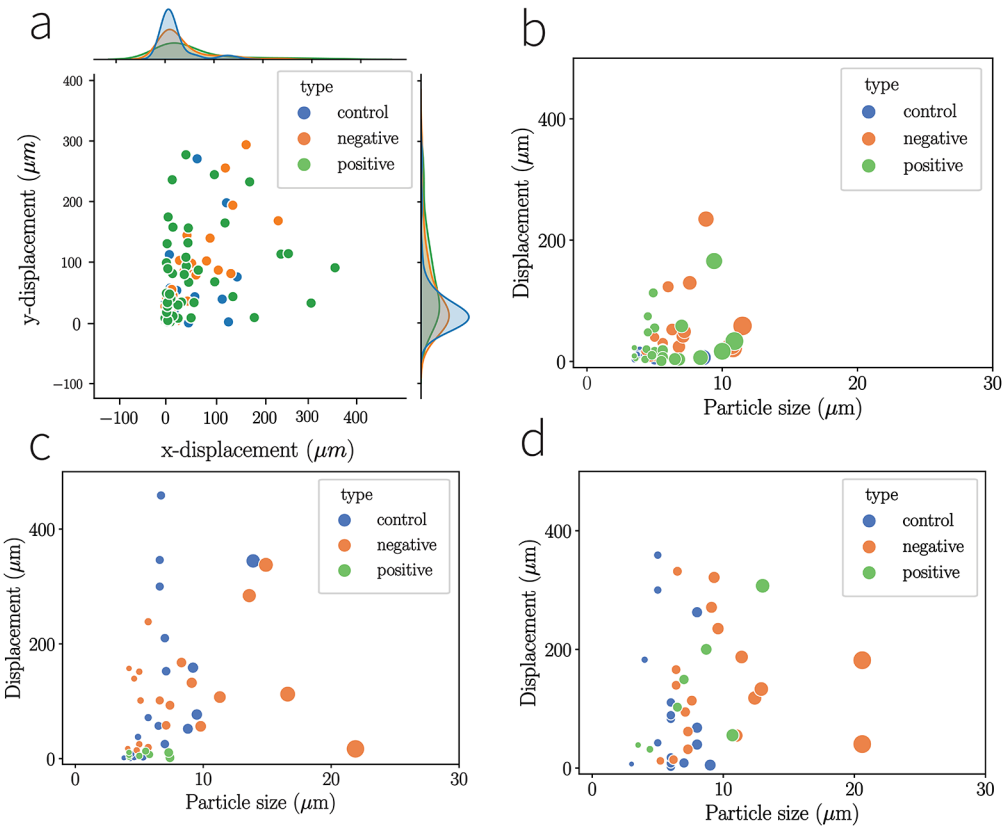

Figure 4. (a) Particle displacements along the *x* and *y* axis on hydrophilic, hydrophobic, and amine-functionalized glass. (b–d) Corresponding size of the particle and distance traveled before adhering to (b) hydrophilic, (c) hydrophobic, and (d) TMA-functionalized glass.

amounted to $\sim -7.5 \times 10^{-10}$, -8.5×10^{-10}, and 7.5×10^{-10} nC per particle for bare, hydrophobic, and amine-functionalized particles, respectively, assuming a particle size of 2.5 μm (see later for microscopic analysis). Molecular models of bare, hydrophobic, and amine-functionalized silica are also shown in Figure S2. Bare particles, hydrophobic particles, and TMA-functionalized particles will be termed control, negative, and positively charged particles, respectively, in this article.

The optical images containing a droplet in contact with the surface during the water contact angle measurements are shown in Figure S3. Hydrophilic glass had a contact angle of 25°, while the hydrophobic glass had a contact angle of 102°, and TMA-functionalized glass was slightly hydrophobic in nature, with a contact angle hovering around 88°. The surface energy of the treated surfaces was calculated based on the water contact angle using the equation below

$$\frac{\cos\ \theta + 1}{2} = \gamma_A(e^{-\beta(\gamma_B - \gamma_A)^2})$$

where θ is the water contact angle, γ_A the surface energy of the solid substrate, γ_B surface energy of water, and β is 0.0001057 $(m^2\ mj^{-1})^2$.[34] The surface energy for hydrophilic glass was calculated to be ~0.9 mN/m, for TMA-treated glass ~0.5 mN/m, and for hydrophobic glass ~0.4 mN/m.

To confirm the coating on glass, XPS analysis was performed, and the corresponding spectra are shown in Figures S4 and S5. All the samples exhibited the expected presence of C, Si, and O as seen in the survey spectra of hydrophobic glass (Figure S4) and TMA-treated glass (Figure S5). For hydrophobic glass, there were five peaks corresponding to C (284.5 eV), C−C (283.9 eV), C−O (288 eV), CF_2(290.9 eV), and CF_3(293.3 eV) as seen in Figure S4b. Two peaks were observed in the detailed Si scans for the hydrophobic glass. The peak at ~102.8 eV corresponds to the silane and that at ~103.5 eV was assigned to SiO_2 as shown in Figure S4c. In Figure S4d, two types of oxygens were present in abundance and could be assigned to the different bonding modes of O in glass. Finally, Figure S4e shows a detailed F scan; a single peak was present at 687.63 V and was assigned to F in the $-CF_2-$ moieties. This confirms the hydrophobic coating on glass. The XPS survey spectrum of TMA-treated glass is shown in Figure S5a; the detailed C spectrum in Figure S5b shows adventitious C (284.5 eV) and C−O (286.6 eV) and another peak at 288.6 eV was assigned to the C−N bond. The detailed Si spectrum shown in Figure S5c shows two peaks at ~102.8 and 103.5 eV due to silane and SiO_2, respectively. The O 1s region shown in Figure S5d has two peaks assigned to different bonding modes in glass. Finally, the TMA-treated glass has a peak at ~399.6 eV that is assigned to the C−N bond.

A digital photograph from the camera is shown in Figure S6a. From this, a small region is selected as seen in Figure S6b. From the image sequences from time-dependent imaging, the region of interest (ROI) was selected and cropped. The photographs in which particles enter the frame were chosen and cropped to comprehend particle motion as they attach to the surface. These cropped images were further analyzed using the "trackpy" module in Python to estimate the movements in the *x*- and *y*-axes.

https://doi.org/10.1021/acs.langmuir.3c01856
Langmuir XXXX, XXX, XXX−XXX

Images of glass slides after particle deposition are shown in Figure 3, wherein Figure 3a represents the hydrophilic glass when positively charged particles adhered to it after 16 s. An ROI in Figure 3a (shown by the dashed rectangle) was chosen where the particle (indicated by the dotted circle) traveled from the top and was attached to the surface. Corresponding pictures are displayed in Figure 3a. The blurring of the particle in the first three images (the first image shows a clean region before the particle appears) shows that the particle was traveling from a depth and as it got adhered, it came into focus. In the image, just as the particle appears in the ROI, i.e., first appearance of a diffused region, a time of 0 ms is assigned. At the end of 180 ms, the particle is moving and slowly coming to focus and finally adheres to the hydrophilic glass at ∼300 ms, and no further change is observed. A video depicting the particle adhesion on glass is shown in Video S1. In Figure 3b, interaction of control particles on a hydrophilic glass substrate was captured, and the inset shows a control particle adhering to the surface without any motion in the $x-y$ direction. The control particle adheres much faster, taking ∼80 ms to adhere to the glass and no further change is seen. Similarly, Figure 3c shows the interaction of negatively charged particles with the hydrophilic glass slides; the inset shows a positively charged particle moving toward the surface as it focuses on the site of adhesion. Furthermore, the negatively charged particle takes ∼50 ms to adhere to the glass. A video showing a particle traveling from the depth and adhering to the glass is shown in Video S2.

The interactions of positively charged particles with hydrophobic glass are shown in Figure S7a and the ROI, representing a particle (shown in a dotted circle) that reached the surface from a certain depth. It took ∼30 ms to adhere to the surface. We observed that the control particle takes a parabolic path to adhere to the hydrophobic glass, as seen in the inset of Figure S7b. The blurriness of the particle as it travels from the depth is prominent at the frame of 120 ms, as shown in the inset, and finally, it comes to focus as it adheres to the surface at the end of ∼200 ms. The interaction of negatively charged particles with the hydrophobic glass is shown in Figure S7c and the inset magnifies the region where the particle adheres to the surface. In the case of the negatively charged particle, we also observed a motion in the x and y directions while traveling from a depth. It took ∼86 ms for it to adhere to the surface.

The interaction between positively charged particles with TMA-functionalized glass is shown in Figure S8a, where a positively charged particle was seen to move along the y direction and adhere to the surface. In this sequence of images, we observed that the particle in focus suddenly moves to a different location, finally adhering to a different location, and it takes ∼480 ms for adhesion. The interaction of the control particle with the TMA-functionalized surface is shown in Figure S8b and the inset shows a particle initially moving toward the surface as it deblurs. Direct adhesion on the surface was observed for negatively charged particles interacting with the TMA-functionalized glass, as seen in Figure S8c (inset).

Due to the boundary layer phenomenon, as the particles are approaching the surface, they would have the least velocity, and the electrostatic forces of attraction/repulsion would dominate. A summary of the particle displacements along different functionalized glasses is shown in Figure 4a. Time-resolved high-speed optical imaging revealed that most particles were displaced by ∼40 and ∼80 μm in the x and y directions before adhering to the surface. The average displacement of control particles was minimal compared to others.

Some outliers showed displacements of up to 140 and 300 μm along the x and y axes, respectively. Based on the above observations, it is apparent that lesser particle movement along the x and y axes is due to "faster" adherence to surfaces with high surface energy. The negatively charged particle of size ∼10 μm traveled the longest distance of ∼230 μm, before colliding with the glass substrate and adhering to the hydrophilic surface, as shown in Figure 4b. Due to the high surface energy of hydrophilic glass, particles witnessed lesser displacement.

Also, we suspect that the positively charged particles had lesser displacement due to electrostatic attraction with the oppositely charged functionalities present on the glass substrate. All positively charged particles traversed less than ∼13 μm before colliding with the hydrophobic glass (Figure 4c). In the case of control and negatively charged particles, the distribution of displacements across the particle size regime was random and no systematic correlation was observed (Figure 4c,d). This could be due to the particle−substrate electrostatic repulsion and steric hindrance offered by the surface groups, which resulted in longer displacements, irrespective of the nature of the charge on the particles. This was evident when the particles adhered to the surface, as shown in Figure S9. All the particles readily adhered to the hydrophilic glass slide, with positively charged particles taking ∼0.054 s to adhere. There was an increase in the time for adhesion to the hydrophobic and TMA-functionalized glass. Particle adhesion took the longest, ∼ 0.45 s, on a TMA-functionalized glass surface. Further experiments are needed to determine the effects of the surface charge and surface energy on the particle−substrate interaction.

Ex situ deposition of particles on glass after 19 s of exposure to model dust particles gave a distribution, as shown in Figure S10. In the case of hydrophilic glass with −OH functionalization, control particles displayed ∼1.8-fold and ∼3-fold higher deposition compared to positively charged and negatively charged particles. In the case of TMA-functionalized glass, control particles exhibited ∼3.5-fold and ∼2.3-fold higher deposition compared to positively charged and negatively charged particles, respectively. In the case of hydrophobic glass with PTFS-functionalization, control particles showed ∼1.6-fold higher deposition than negatively charged particles. However, the highest fouling was by positively charged particles. We suspect that the highest fouling was due to an opposite surface charge between the positively charged particles and hydrophobic glass. This implies that surface functionalization of the glass substrate results in lesser particle deposition or fouling. The highest fouling was observed with the hydrophilic glass slide having −OH functionalization. Further studies are needed to study the influence of surface charge and energy dependencies on the fouling of glass by real dust.

Exposure to Ambient Dust. To investigate the impact of surface functionalization on ambient dust deposition, chemically treated glass slides were placed at a height of ∼20 m from the floor of our laboratory building within the IIT Madras campus and were viewed with an optical microscope at the end of 4 days. Particle size was measured using the Feret diameter feature in ImageJ and the size distribution is shown in Figure S11. At the end of the fourth day, particle deposition increased,

https://doi.org/10.1021/acs.langmuir.3c01856
Langmuir XXXX, XXX, XXX−XXX

as seen for hydrophilic glass slides. Dust particles of 60 μm in size were observed at the end of 4 days. Hydrophobic glass slides fouled less compared to hydrophilic glass with a maximum particle size of 100 μm. TMA-functionalized glass fouled the least even at the end of 4 days. Lower surface energy and long-chain moieties on the surface of the glass could reduce fouling. Prolonged exposure to ambient dust would provide further quantifiable data on the overall reduction in fouling based on surface functionalization. However, this is further dependent on many experimental conditions, and the outcomes will be dependent on local factors such as humidity, temperature, particulate matter concentration, and wind velocity.

Ease of Cleaning the Surface. We placed fine sand particles on hydrophilic, hydrophobic, and TMA-treated glass, on which water droplets were placed. We observed that the droplet was spread on hydrophilic glass (Figure S12a) but it retained the shape in the case of functionalized glass as shown in Figure S12b,c. The surface functionalization did reduce the surface energy, which enabled the droplet to retain the droplet form. There was significant pinning of droplets when the slides were tilted as seen in Figure S12d–f.

CONCLUSIONS

Ambient dust exposure on chemically functionalized glass surfaces showed that TMA-functionalized and hydrophobic glass surfaces fouled the least compared to the hydrophilic glass. An experimental setup was designed to observe particle adhesion on model glass surfaces in situ. Particle motion along these surfaces was tracked successfully with a high-speed camera. The hydrophilic glass surface fouled more readily due to particle deposition. Deposition on such a surface was immediate (within 0.05 s), and the least lateral motion of the particles (2.3 μm) was observed. Also, positively charged particles adhered on a hydroxylated glass in ∼0.054 s as opposed to 0.40 and 0.45 s needed for adhesion on a TMA-functionalized and a hydrophobic glass, respectively. These observations could shed light on the interaction of microscopic particles on surfaces. In addition, varying the %RH while performing the experiments can induce condensation on the glass, affecting particle adhesion, and we suspect easier particle adhesion on the glass. The presence of droplets on the glass could lead to the formation of a coffee ring of dust particles upon drying. By combining surface functionalization with the electrostatic surface cleaning method shown by Panat and Varanasi, we expect that the overall DC potential needed for cleaning the soiled surfaces could be reduced greatly. By reducing the surface energy, the centrifugal force needed to dislodge particles on glass could be reduced. In the future, we plan to study the effect of carbon chain length on the adhesion time of the particles. In situ particle deposition coupled with charge measurement is being planned and would provide exact information about the surface charge and surface energy.

ASSOCIATED CONTENT

Supporting Information

The Supporting Information is available free of charge at https://pubs.acs.org/doi/10.1021/acs.langmuir.3c01856.

FTIR spectra of bare, amine, and hydrophobic silica; ambient charge of particles; water contact angle measurements; optical image from the high-speed camera before processing; digital photographs of particle interactions on amine and hydrophobic glass; heat-map representing the time taken for the particles to adhere to different types of glass; and particle size distribution of deposited particles on different types of glass (PDF)

MATLAB code used to calculate the ferret diameter (PDF)

Video depicting particle adhesion on glass (MP4)

Video showing a particle traveling from the depth and adhering to the glass (MP4)

AUTHOR INFORMATION

Corresponding Authors

Ramamurthy Nagarajan − *Department of Chemical Engineering, Indian Institute of Technology Madras, Chennai 600036, India*; Email: nag@iitm.ac.in

Thalappil Pradeep − *DST Unit of Nanoscience and Thematic Unit of Excellence, Department of Chemistry, Indian Institute of Technology Madras, Chennai 600036, India*; orcid.org/0000-0003-3174-534X; Email: pradeep@iitm.ac.in

Authors

Pillalamarri Srikrishnarka − *DST Unit of Nanoscience and Thematic Unit of Excellence, Department of Chemistry, Indian Institute of Technology Madras, Chennai 600036, India; Department of Chemical Engineering, Indian Institute of Technology Madras, Chennai 600036, India*; orcid.org/0000-0001-5187-6879

Dhivyaraja Kumaran − *Department of Applied Mechanics, Indian Institute of Technology Madras, Chennai 600036, India*

Amoghavarsha Ramachandra Kini − *DST Unit of Nanoscience and Thematic Unit of Excellence, Department of Chemistry, Indian Institute of Technology Madras, Chennai 600036, India*

Vishal Kumar − *DST Unit of Nanoscience and Thematic Unit of Excellence, Department of Chemistry, Indian Institute of Technology Madras, Chennai 600036, India; Department of Chemical Engineering, Indian Institute of Technology Madras, Chennai 600036, India*; orcid.org/0000-0002-2374-0568

Ankit Nagar − *DST Unit of Nanoscience and Thematic Unit of Excellence, Department of Chemistry, Indian Institute of Technology Madras, Chennai 600036, India*

Md Rabiul Islam − *DST Unit of Nanoscience and Thematic Unit of Excellence, Department of Chemistry, Indian Institute of Technology Madras, Chennai 600036, India*; orcid.org/0000-0001-6454-4013

Complete contact information is available at: https://pubs.acs.org/10.1021/acs.langmuir.3c01856

Author Contributions

T.P., R.N., and P.S. designed the research. T.P. and R.N. supervised the progress, and P.S. and D.K. performed experiments using the high-speed camera. V.K. measured the ambient charge of the particles; A.M.K., A.K., and M.R.I. assisted in analyzing the results and making figures. The final version of the manuscript was written with the contributions of all authors.

Notes

The authors declare no competing financial interest.

https://doi.org/10.1021/acs.langmuir.3c01856
Langmuir XXXX, XXX, XXX−XXX

■ ACKNOWLEDGMENTS

The authors thank Prof. Mahesh Panchagnula for allowing us to use his high-speed camera. The authors acknowledge Prof. Pijush Ghosh for contact angle measurements. The authors thank the "Dust free glass" project funded by Saint Gobain Research India Ltd. We thank Dr. B S. Srinivas Prasad for his valuable suggestions throughout the project. T.P. acknowledges funding from the Centre of Excellence on Molecular Materials and Functions under the Institute of Eminence scheme of IIT Madras. P.S. would like to thank Paulami Bose for assisting in drawing the molecular structures. P.S., D.K., V.K., and A.K. thank IIT Madras for their research fellowship. A.M.K and M.R.I. thank the Council of Science and Industrial Research (CSIR), Government of India for their research fellowship.

■ REFERENCES

(1) van der Does, M.; Knippertz, P.; Zschenderlein, P.; Giles Harrison, R.; Stuut, J.-B. W. The Mysterious Long-Range Transport of Giant Mineral Dust Particles. *Sci. Adv.* **2018**, *4* (12), No. eaau2768.
(2) Elminir, H. K.; Ghitas, A. E.; Hamid, R. H.; El-Hussainy, F.; Beheary, M. M.; Abdel-Moneim, K. M. Effect of Dust on the Transparent Cover of Solar Collectors. *Energy Convers. Manage.* **2006**, *47* (18−19), 3192−3203.
(3) Panat, S.; Varanasi, K. K. Electrostatic Dust Removal Using Adsorbed Moisture-Assisted Charge Induction for Sustainable Operation of Solar Panels. *Sci. Adv.* **2022**, *8* (10), No. eabm0078.
(4) Sarver, T.; Al-Qaraghuli, A.; Kazmerski, L. L. A Comprehensive Review of the Impact of Dust on the Use of Solar Energy: History, Investigations, Results, Literature, and Mitigation Approaches. *Renewable Sustainable Energy Rev.* **2013**, *22*, 698−733.
(5) Moon, S. M.; Shin, C. Y.; Huh, J.; Oh, K. W.; Hong, D. Window Cleaning System with Water Circulation for Building Façade Maintenance Robot and Its Efficiency Analysis. *Int. J. Precis. Eng. Manuf. - Green Technol.* **2015**, *2* (1), 65−72.
(6) Moffet, R. C.; Desyaterik, Y.; Hopkins, R. J.; Tivanski, A. V.; Gilles, M. K.; Wang, Y.; Shutthanandan, V.; Molina, L. T.; Abraham, R. G.; Johnson, K. S.; Mugica, V.; Molina, M. J.; Laskin, A.; Prather, K. A. Characterization of Aerosols Containing Zn, Pb, and Cl from an Industrial Region of Mexico City. *Environ. Sci. Technol.* **2008**, *42* (19), 7091−7097.
(7) Chen, H.; Laskin, A.; Baltrusaitis, J.; Gorski, C. A.; Scherer, M. M.; Grassian, V. H. Coal Fly Ash as a Source of Iron in Atmospheric Dust. *Environ. Sci. Technol.* **2012**, *46* (4), 2112−2120.
(8) McGaughey, G. R.; Desai, N. R.; Allen, D. T.; Seila, R. L.; Lonneman, W. A.; Fraser, M. P.; Harley, R. A.; Pollack, A. K.; Ivy, J. M.; Price, J. H. Analysis of Motor Vehicle Emissions in a Houston Tunnel during the Texas Air Quality Study 2000. *Atmos. Environ.* **2004**, *38* (20), 3363−3372.
(9) Huang, L.; Zhu, Y.; Wang, Q.; Zhu, A.; Liu, Z.; Wang, Y.; Allen, D. T.; Li, L. Assessment of the Effects of Straw Burning Bans in China: Emissions, Air Quality, and Health Impacts. *Sci. Total Environ.* **2021**, *789*, 147935.
(10) Ke, C.; Zhang, C.; Wu, X.; Jiang, Y. Highly Transparent and Robust Superhydrophobic Coatings Fabricated via a Facile Sol-Gel Process. *Thin Solid Films* **2021**, *723*, 138583.
(11) Liu, Y.; Tan, X.; Li, X.; Xiao, T.; Jiang, L.; Nie, S.; Song, J.; Chen, X. Eco-Friendly Fabrication of Transparent Superhydrophobic Coating with Excellent Mechanical Robustness, Chemical Stability, and Long-Term Outdoor Durability. *Langmuir* **2022**, *38* (42), 12881−12893.
(12) Yu, S.; Guo, Z.; Liu, W. Biomimetic Transparent and Superhydrophobic Coatings: From Nature and beyond Nature. *Chem. Commun.* **2015**, *51* (10), 1775−1794.
(13) Helmer, D.; Keller, N.; Kotz, F.; Stolz, F.; Greiner, C.; Nargang, T. M.; Sachsenheimer, K.; Rapp, B. E. Transparent, Abrasion-Insensitive Superhydrophobic Coatings for Real-World Applications. *Sci. Rep.* **2017**, *7* (1), 15078.
(14) Wu, Y.; Tan, X.; Wang, Y.; Tao, F.; Yu, M.; Chen, X. Nonfluorinated, Transparent, and Antireflective Hydrophobic Coating with Self-Cleaning Function. *Colloids Surf., A* **2022**, *634*, 127919.
(15) Allahdini, A.; Jafari, R.; Momen, G. Transparent Non-Fluorinated Superhydrophobic Coating with Enhanced Anti-Icing Performance. *Prog. Org. Coat.* **2022**, *165*, 106758.
(16) Jeevajothi, K.; Subasri, R.; Soma Raju, K. R. C. Transparent, Non-Fluorinated, Hydrophobic Silica Coatings with Improved Mechanical Properties. *Ceram. Int.* **2013**, *39* (2), 2111−2116.
(17) Dhar, M.; Kara, U. I.; Das, S.; Xu, Y.; Mandal, S.; Dupont, R. L.; Boerner, E. C.; Chen, B.; Yao, Y.; Wang, X.; Manna, U. Design of a Self-Cleanable Multilevel Anticounterfeiting Interface through Covalent Chemical Modulation. *Mater. Horiz.* **2023**, *10* (6), 2204−2214.
(18) Zhang, J.; Seeger, S. Superoleophobic Coatings with Ultralow Sliding Angles Based on Silicone Nanofilaments. *Angew. Chem., Int. Ed.* **2011**, *50* (29), 6652−6656.
(19) Ganesh, V. A.; Dinachali, S. S.; Nair, A. S.; Ramakrishna, S. Robust Superamphiphobic Film from Electrospun TiO2 Nanostructures. *ACS Appl. Mater. Interfaces* **2013**, *5* (5), 1527−1532.
(20) Ganesh, V. A.; Nair, A. S.; Raut, H. K.; Yuan Tan, T. T.; He, C.; Ramakrishna, S.; Xu, J. Superhydrophobic Fluorinated POSS-PVDF-HFP Nanocomposite Coating on Glass by Electrospinning. *J. Mater. Chem.* **2012**, *22* (35), 18479−18485.
(21) Ganesh, V. A.; Dinachali, S. S.; Raut, H. K.; Walsh, T. M.; Nair, A. S.; Ramakrishna, S. Electrospun SiO 2 Nanofibers as a Template to Fabricate a Robust and Transparent Superamphiphobic Coating. *RSC Adv.* **2013**, *3* (12), 3819−3824.
(22) Bouaddi, S.; Fernández-García, A.; Sansom, C.; Sarasua, J. A.; Wolfertstetter, F.; Bouzekri, H.; Sutter, F.; Azpitarte, I. A Review of Conventional and Innovative- Sustainable Methods for Cleaning Reflectors in Concentrating Solar Power Plants. *Sustainability* **2018**, *10* (11), 3937.
(23) Sun, D.; Böhringer, K. F. An Active Self-Cleaning Surface System for Photovoltaic Modules Using Anisotropic Ratchet Conveyors and Mechanical Vibration. *Microsyst. Nanoeng.* **2020**, *6* (1), 87.
(24) Varga, H. F.; Wiesner, M. R. Relationship between Atomic Force Microscopy and Centrifugation Measurements for Dust Fractions Implicated in Solar Panel Soiling. *Environ. Sci. Technol.* **2022**, *56* (13), 9604−9612.
(25) Kawamoto, H. Electrostatic Cleaning Equipment for Dust Removal from Soiled Solar Panels. *J. Electrost.* **2019**, *98*, 11−16.
(26) Wang, P.; Wang, H.; Li, J.; Ni, L.; Wang, L.; Xie, J. A Superhydrophobic Film of Photovoltaic Modules and Self-Cleaning Performance. *Sol. Energy* **2021**, *226*, 92−99.
(27) Zhang, Y.; Gong, X. Smart and Durable pH-Responsive Superhydrophobic Fabrics with Switchable Surface Wettability for High-Efficiency and Complex Oil/Water Separation. *Giant* **2023**, *14*, 100157.
(28) Yu, H.; Wu, M.; Duan, G.; Gong, X. One-Step Fabrication of Eco-Friendly Superhydrophobic Fabrics for High-Efficiency Oil/Water Separation and Oil Spill Cleanup. *Nanoscale* **2022**, *14* (4), 1296−1309.
(29) Xiong, Z.; Yu, H.; Gong, X. Designing Photothermal Superhydrophobic PET Fabrics via In Situ Polymerization and 1,4-Conjugation Addition Reaction. *Langmuir* **2022**, *38* (28), 8708−8718.
(30) Liu, Y.; Sheng, Z.; Huang, J.; Liu, W.; Ding, H.; Peng, J.; Zhong, B.; Sun, Y.; Ouyang, X.; Cheng, H.; Wang, X. Moisture-Resistant MXene-Sodium Alginate Sponges with Sustained Superhydrophobicity for Monitoring Human Activities. *Chem. Eng. J.* **2022**, *432*, 134370.
(31) Wang, X.; Liu, Y.; Cheng, H.; Ouyang, X. Surface Wettability for Skin-Interfaced Sensors and Devices. *Adv. Funct. Mater.* **2022**, *32* (27), 2200260.
(32) Liu, Y.; Li, X.; Yang, H.; Zhang, P.; Wang, P.; Sun, Y.; Yang, F.; Liu, W.; Li, Y.; Tian, Y.; Qian, S.; Chen, S.; Cheng, H.; Wang, X. Skin-Interfaced Superhydrophobic Insensible Sweat Sensors for Evaluating

https://doi.org/10.1021/acs.langmuir.3c01856
Langmuir XXXX, XXX, XXX−XXX

Body Thermoregulation and Skin Barrier Functions. *ACS Nano* **2023**, *17* (6), 5588−5599.
(33) Thomas Iii, S. W.; Vella, S. J.; Dickey, M. D.; Kaufman, G. K.; Whitesides, G. M. Controlling the Kinetics of Contact Electrification with Patterned Surfaces. *J. Am. Chem. Soc.* **2009**, *131* (25), 8746−8747.
(34) Gindl, M.; Sinn, G.; Gindl, W.; Reiterer, A.; Tschegg, S. A Comparison of Different Methods to Calculate the Surface Free Energy of Wood Using Contact Angle Measurements. *Colloids Surf., A* **2001**, *181* (1−3), 279−287.

https://doi.org/10.1021/acs.langmuir.3c01856
Langmuir XXXX, XXX, XXX−XXX